Volume 11
Number 42
14 November 2020
Pages 11355–11634

Chemical Science

rsc.li/chemical-science

ISSN 2041-6539

ROYAL SOCIETY OF CHEMISTRY

EDGE ARTICLE

Chung-Hang Leung, Dik-Lung Ma *et al.*
Structure-guided discovery of a luminescent theranostic toolkit for living cancer cells and the imaging behavior effect

Chemical Science

ROYAL SOCIETY OF CHEMISTRY

EDGE ARTICLE

View Article Online
View Journal | View Issue

Cite this: *Chem. Sci.*, 2020, **11**, 11404

All publication charges for this article have been paid for by the Royal Society of Chemistry

Structure-guided discovery of a luminescent theranostic toolkit for living cancer cells and the imaging behavior effect†

Chun Wu,‡[a] Ke-Jia Wu,‡[b] Jin-Biao Liu, ‡[ac] Wanhe Wang, [a] Chung-Hang Leung *[b] and Dik-Lung Ma *[a]

Dual-functional theranostics are powerful tools that can allow for the in-field understanding of cancer pathology, yet their use is held back by the paucity of suitable theranostics for living systems. Moreover, typical *in vitro* screening conditions for probe molecules do not necessarily generate candidates that can function effectively in the natural *in cellulo* environment, limiting their follow-up use in living systems. We introduce herein a general strategy for the development of an iridium(III) theranostic by grafting a well-known inhibitor as a "binding unit" onto an iridium(III) complex precursor as a "signaling unit". To further optimize their emissive properties, we explored the effect of imaging behavior by incorporating different substituents onto the parental "signaling unit". This design concept was validated by a series of tailored iridium(III) theranostics **2a–2h** for the visualization and inhibition of EGFR in living cancer cells. By comprehensively assessing the theranostic potency of **2a–2h** in both *in vitro* and *in cellulo* contexts, probe **2f** containing electron-donating methoxy groups on the "signaling unit" was discovered to be the most promising candidate theranostic with desirable photophysical/chemical properties. Probe **2f** selectively bound to EGFR *in vitro* and *in cellulo*, enabling it to selectively discriminate living EGFR-overexpressing cancer cells from normal cells that express low levels of EGFR with an "always-on" luminescence signal output. In particular, its long-lived lifetime enabled its luminescence signal to be readily distinguished from the interfering fluorescence of organic dyes by using time-resolved techniques. Complex **2f** simultaneously visualized and inhibited EGFR in a dose-dependent manner, leading to a reduction in the phosphorylation of downstream proteins ERK and MEK, and inhibition of the activity of downstream transcription factor AP1. Notably, complex **2f** is comparable to the parental EGFR inhibitor **1b**, in terms of both inhibitory activity against EGFR and cytotoxicity against EGFR-overexpressing cancer cells. This tailored dual-functional iridium(III) theranostic toolkit provides an alternative strategy for the personalized diagnosis and treatment of cancers.

Received 20th August 2020
Accepted 23rd September 2020

DOI: 10.1039/d0sc04576d

rsc.li/chemical-science

Introduction

The combination of an imaging agent and a therapeutic drug into a single molecular entity is known as "theranostics", and has emerged as a powerful technique used for the timely and personalized monitoring of cancer cells.[1,2] Theranostic strategies provide remarkable advantages over conventional probes or drugs as they enable the suppression of specific diseases while simultaneously realizing the *in situ* detection of the therapeutic dynamics, metabolic pathway, biodistribution or delivery pharmacokinetics of the drug.[3] Moreover, the elimination of an additional imaging agent or inhibitor can not only largely simplify the administration process, but also significantly reduce the potential of undesired dose mismatch or drug–drug crosstalk between the imaging agent and therapeutic drug.[4] However, it has proven difficult to design synthetic theranostic toolkits tailored for specialized purposes, particularly for the monitoring of targeted analytes in living systems.

A desirable theranostic molecule for cancer cells needs to possess biological activity as an inhibitor while simultaneously maintaining the photophysical/chemical properties of a probe. One of the most popular strategies for the development of theranostic agents uses nanomaterials to incorporate drug component and probe component.[3,5–7] However, these strategies suffer from limited biocompatibility since the nanomaterial-based platforms generally have larger sizes, with

[a]*Department of Chemistry, Hong Kong Baptist University, Kowloon, Hong Kong SAR 999077. E-mail: edmondma@hkbu.edu.hk*

[b]*Institute of Chinese Medical Sciences, State Key Laboratory of Quality Research in Chinese Medicine, University of Macau, Taipa, Macau SAR 999078. E-mail: duncanleung@um.edu.mo*

[c]*School of Metallurgical and Chemical Engineering, Jiangxi University of Science and Technology, Ganzhou, China*

† Electronic supplementary information (ESI) available. See DOI: 10.1039/d0sc04576d

‡ The authors contribute equally in this work.

their dimensions up to 100 nm.[8–12] An additional drawback of nanomaterial-based theranostic platforms is that the drug and probe components are sometimes still technically separate entities that are simply loaded onto the core/shell regions of the nanomaterial.[6,13,14] An alternative and simpler strategy for theranostic has been explored, based on using pure organic scaffolds or metal–organic integrated complexes. Compared to nanomaterials, small molecule-based theranostic agents are more compact and simpler in structure, which confers high reproducibility as well as allowing easy modification of molecular structures to achieve the desired photochemical property, selectivity, biocompatibility, therapeutic activity, cellular uptake efficiency and/or drug excretion with reduced side effects.[15–20]

Fluorescent dyes, while widely used in theranostic agents, suffer from several defects including high photobleaching rate, short-lived lifetime and low signal-to-noise ratios in the highly autofluorescent cellular environment, which extensively limits their in-field utilization in the complicated biological systems.[21,22] In contrast, metal–organic small molecule theranostics have opened up new possibilities for the *in situ* simultaneous visualization and inhibition of cancer cells due to their advantageous photophysical properties (*e.g.* long-lived phosphorescence lifetime, high quantum yield, large Stokes shift, *etc.*)[23–27] and the easily tunable nature of their photophysical/chemical properties.[28] For example, lanthanide-based complexes (*i.e.* europium(III), terbium(III), ytterbium(III) complexes) are endowed with typical two-photon excitation behaviour and offer facile discrimination of their signal output with emission bands spanning from visible to near-infrared (NIR) ranges, allowing for deep penetration in biological system.[29] Meanwhile, transition metal complex-based strategies (*i.e.* iridium(III) complex) are relatively photostable compared to most organic fluorophores such as commercially available organic dye DAPI (DAPI = 4′,6-diamidino-2-phenylindole), enabling their favoured applications in long-term observation and dynamic monitoring of the targeted analytes in living biological system.[30,31] Encouragingly, metal complexes (including iridium(III), ruthenium(III), platinum(IV) and gold(III) complexes) have been developed as for simultaneous imaging and treatment of cancers, suggesting their great potential as theranostic agents.[15,32–35]

Epidermal growth factor receptor (EGFR) is a well-known protein tyrosine kinase that plays a crucial role in the pathology of various cancers.[36,37] The *in situ* monitoring of the abnormal overexpression of EGFR in living cancer cells can allow for the timely treatment, diagnosis and assessment of the onset, recurrence, tolerance, efficiency and/or toxicity for cancers. However, small molecule-based EGFR-specific theranostics, particularly those based on long-lifetime transition metal complexes capable for dynamic monitoring in living systems, remain poorly explored. Moreover, typical *in vitro* screening conditions for probe molecules do not necessarily generate candidates that can function effectively in the natural *in cellulo* environment, limiting their follow-up use in living systems.[38,39] Given the paucity of suitable long-lived theranostic toolkits for the specific targeting of EGFR, we intended to validate our design concept by constructing a series of tailored iridium(III) theranostic agents for the simultaneous visualization and inhibition of EGFR in living cancer cells, which were verified using both *in vitro* and *in cellulo* screens (Scheme 1).

One key challenge in the design of a transition metal complex-based theranostic agent is being able to acquire biological activity against the target, while retaining desirable photophysical/chemical properties for the imaging of living cells. Poor selectivity of the theranostic towards cancer cells can lead to undesired cytotoxicity against surrounding healthy cells.[40] Another challenge that has to be overcome is the fact that many transition metal complexes exhibit strong emission and good stability only in organic solvents, and do not function well in aqueous solutions, such as cellular environment.[41] Meanwhile, a red-shifted luminescence is generally the most preferred emission range in order to avoid interference from the autofluorescence, light scattering and/or optical absorption in the cellular environment.[42] Moreover, an "always-on" or "switch-on" emission profile is more desirable compared with a "switch-off" detection mode as this increases the accuracy in the discrimination of cancer cells from healthy cells, and/or in the report of the biological events.[32,43,44] Finally, the ability of the candidate theranostics to accumulate at the targeted locations (*e.g.* cytoplasm and/or organelles) in living cells should also be considered, as this could largely limit their use for the monitoring of living cells.[45,46]

To overcome these problems, this design strategy takes advantage of the tunable photophysical/chemical properties of the transition metal complex precursor **1a** (Fig. S1†). A well-known EGFR inhibitor **1b**, with high selectivity and inhibition activity against EGFR,[47] is introduced to the tailored metal complex. Generally, an assembled metal complex-based theranostic agent consists of a "binding unit" that selectively binds to the targeted analyte with desired biological activity, a "signaling unit" that illuminates the targeted analytes by transducing the sensing event into a dynamic luminescent signal output, and a "linker" that tethers the binding unit and signaling unit into

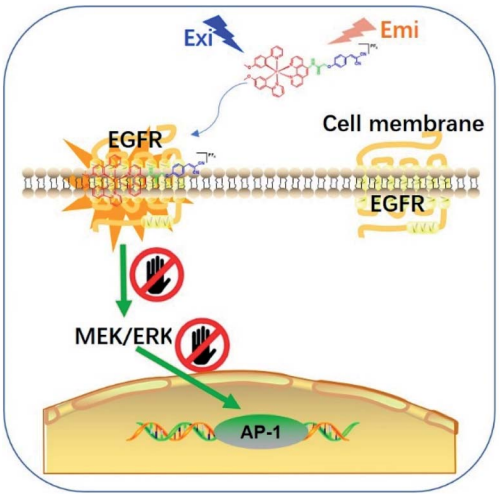

Scheme 1 Schematic diagram showing the *in situ* tracking and suppression of EGFR using a smart and tailored iridium(III) theranostic toolkit.

an integrated molecule (Fig. 1). In this study, the "binding unit" is the EGFR-targeting drug moiety **1b**, which is expected to confer high selectivity and inhibition activity against EGFR. The final complexes **2a–2h** thus all contain an EGFR-targeting moiety **1b** grafted onto the N^N ligand of the parent iridium(III) scaffold **1a**. To further optimize the emissive behavior of the signaling parent metal complex precursor **1a**, we explored the effect of incorporating different substituents such as electron-withdrawing fluorine atoms (**2e**), electron-donating methyl (**2g**) or methoxy (**2f**) groups, different aromatic ring systems (**2a–2d**) or a sulfur-containing heterocycle (**2h**). The lead candidate was comprehensively screened by assessment of both *in vitro* and *in cellulo* performance. The aim was to obtain a theranostic that retained biological activity while possessing suitable phosphorescence lifetime, quantum yield, Stokes shift, and absorbance and/or emission profiles in living system.

Results and discussion

To synthesize the iridium(III) complex-based theranostic molecules, the reference inhibitor **1b** was initially attached to the parent complex precursor **1a** (Fig. S1†) *via* two different strategies, either by directly conjugation to the N^N ligand of parent complex **1b** (synthesis route 1, Scheme S1†) or a linker tethered parent complex **S5** (synthesis routes 2 and 3, Scheme S1†). Unfortunately, synthesis route 1 proceeded poorly owing to the unsatisfactory yield and solubility of the EGFR binding moiety-containing N^N ligand **S4**. Attempted optimization of the type and amount of the catalyst, alkali, and reaction solvent system failed to produce the desired product. In the next attempt, we switched to an alternative strategy by directly attaching the binding moiety to the parent complex precursor **1a.** Complex **1a** was first tethered by a linker to obtain an intermediate complex **S6**. However, complex **S6** and **1b** showed quite different solubilities in various organic solvents (*e.g.* ethanol, methanol, acetonitrile and dichloromethane, *etc.*). Hence, the direct conjugation of the binding moiety **1b** to **S6** proceeded poorly with many side products either in single solvent or mixed solvent system, causing problems with the subsequent purification process. To address this problem, the conjugation of the targeted **1b** moiety was therefore divided into two separate steps, involving an initial substitution of the **S1** moiety to give **S7**, and the subsequent Knoevenagel condensation of propanedinitrile. Encouragingly, this alternative strategy produced much fewer impurities and the yield of the final complex **2a** (Fig. 1) could then be further improved by optimization of the reaction temperature, and type and amount of alkali, catalyst and organic solvents involved in the process. The iridium(III) analogues **2b–2h** were synthesized in similar fashion *via* the intermediate parent complex **1a**. Complexes **2a–2h** were characterized by ^{1}H NMR, ^{13}C NMR, high-resolution mass spectrometry (HRMS) and high performance liquid chromatography (HPLC) techniques (Fig. S2†).

We first examined the *in vitro* inhibition efficiency of iridium(III) complexes **2a–2h** against EGFR activity (Fig. 2a), utilizing a commercially available EGFR kinase assay kit. EGFR inhibitor **1b** was employed as a reference drug. Excitingly, these complexes displayed 20–50% enhanced EGFR inhibition compared to the drug precursor **1b**, which was attributed to the interaction of the drug precursor and the parent iridium(III) complex precursor to form a more biologically active entity. Among these conjugates, **2g** bearing methyl groups on its C^N

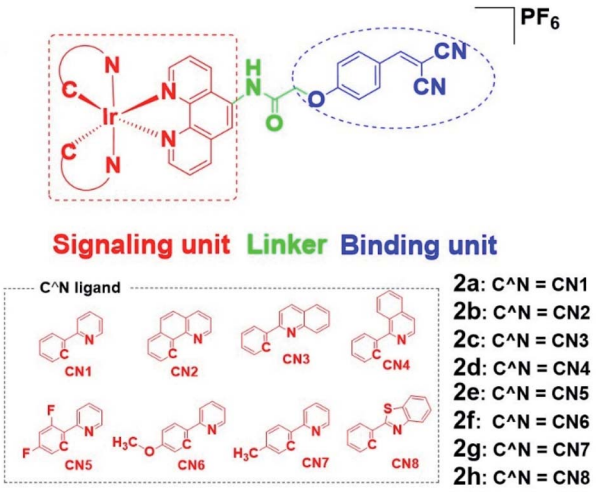

Fig. 1 Design principle of EGFR-targeting theranostic agents **2a–2h** and chemical structures of the library of auxiliary C^N ligands used for fine-tuning the photo-physical/-chemical property of the parent iridium(III) complex precursor **1a**.

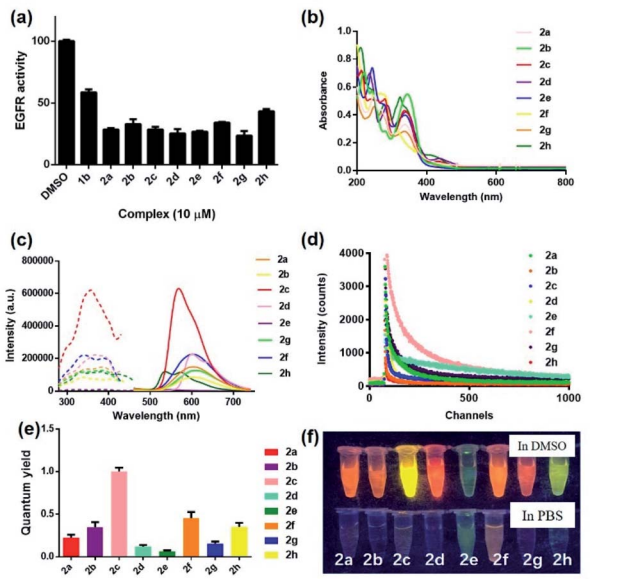

Fig. 2 (a) Inhibition activity of complexes **2a–2h** and reference EGFR inhibitor **1b** (10 μM) against EGFR (10 μg mL^{-1}) as measured by a fluorescence-based kinase assay. The fluorescence intensity was detected at ex/em = 330 nm/450 nm. (b) Absorbance spectra of complexes **2a–2h** (5 μM) in ACN. (c) Excitation and emission spectra of complexes **2a–2h** (5 μM) in DMSO. (d) Emission decay curves of complexes **2a–2h** (5 μM) in PBS buffer containing 0.5% DMSO. (e) Quantum yields of complexes **2a–2h** (5 μM). (f) Photographs of complexes **2a–2h** (5 μM) observed under UV light (365 nm) in dimethyl sulfoxide (DMSO) and PBS buffer containing 0.5% DMSO, respectively.

ligands showed the highest inhibitory activity against EGFR, whereas the sulfur heterocycle-containing **2h** showed comparatively the weakest activity. These results suggested that the integration of the drug precursor (**1b**) onto the metal complex core not only retained, but slightly improved the inhibition efficiency against EGFR.

In light of this encouraging result, we next studied the intrinsic photophysical properties of **2a–2h** *in vitro*. Complexes **2a–2h** showed characteristic absorbance bands of transition metal complexes at 208–346 nm in the UV-Vis spectra (Fig. 2b), which can be assigned to the spin-allowed intraligand (^{1}IL) absorption and metal-to-ligand charge-transfer (^{1}MLCT) transition.[48] The maximum emission wavelength of complexes **2a–2h** were mainly located in the range of 529–611 nm (Fig. 2c). The presence of electron-withdrawing fluorine atoms (**2e**) or sulfur-containing heterocyclic ring (**2h**) also lead to a relatively smaller Stokes shifts (198–205 nm) compared to the other six complexes (211–266 nm). Still, all these complexes had Stokes shifts that are much larger than the typical Stokes shift of fluorescent dyes (around 100 nm), thus making them less susceptible to self-quenching. Notably, complex **2c** displayed the strongest luminescence intensity, which might be attributed to subtle variation of the electron density and/or metal-to-ligand-charge-transfer (MLCT) state caused by the joint interplay of the aromatic ring and the π–π conjugation system located in the auxiliary C^N and N^N ligands. Moreover, complexes **2a–2h** all displayed characteristic long-lived lifetimes in sub-microsecond regime[49,50] (Fig. 2d and Table S1†), which are much longer than the typical nanosecond decay times of organic fluorophores. Complexes **2a–2h** exhibited biexponential decay, with the two decay components of each complex showing similar lifetime regimes under the same experimental conditions in PBS buffer containing 0.5% DMSO (Table S1†). The biexponential decay of complexes **2a–2h** is possibly attributed to the presence of two distinct conformations.[33,51,52] The average lifetime of the decay components of complexes containing electron-withdrawing fluorine atoms (**2e**), electron-donating methoxy moieties (**2f**) or sulfur-containing heterocycles (**2h**) displayed comparatively longer lifetimes of 525, 139 and 112 ns, respectively among the group in the PBS buffer containing 0.5% DMSO (Table S1†). These long lifetimes would enable the emission of complexes **2a–2h** to be discriminated from a highly auto-fluorescent background in the complicated cellular environment by use of time-resolved emission spectroscopy (TRES). Additionally, all eight complexes showed comparable (**2d**, **2e** and **2g**) (0.057–0.136) or much higher (**2a**, **2b**, **2c**, **2f** and **2h**) (0.202–0.968) quantum yields compared to the widely-used standard $Ru(bpy)_3$ (bpy = 2,2′-bipyridine) (0.062) (Fig. 2e). Notably, the theranostic agents **2a–2h** (5 μM) exhibited colourful luminescence upon the irradiation of UV light (365 nm) in dimethyl sulfoxide (DMSO) and PBS buffer containing 0.5% DMSO (Fig. 2f and S3†). Complexes containing either electron-withdrawing groups (**2e**) or the sulfur-containing heterocyclic ring (**2h**) on their auxiliary C^N ligands displayed the most blue-shifted emission maxima and appeared blue and green luminescence, respectively, while the other six complexes showed luminescence colors in the yellow or orange region. Overall, these results suggested that the imaging behavior of the iridium(III) theranostic can be fine-tuned by modifying auxiliary functional groups of the parent "signaling unit".

Inspired by the promising luminescent characteristics of complexes **2a–2h**, their practical application as luminescent probes for EGFR imaging in the EGFR-overexpressing A431 human epidermoid carcinoma cell line was next explored (Fig. 3). Living A431 cells were initially incubated with the reference EGFR inhibitor **1b** (1 μM) for 3 h as a competing inhibitor, followed by the addition of probes **2a–2h** (1 μM) for 2 h at 37 °C. Unexpectedly, probe **2f** containing electron-donating methoxy groups on the "signaling unit", rather than the most luminescent counterpart **2c** or the most long-lived counterpart **2d**, displayed the most distinguished luminescence change in the presence and absence of the competition EGFR inhibitor **1b** over the other seven probes as revealed by the confocal assay. This result suggested that **2f** not only enabled the practical detection of EGFR in living A431 cells, but also exhibited better selectivity towards EGFR over the other probes *in cellulo*. In contrast, probe **2g** containing electron-donating methyl groups on the "signaling unit", exhibited negligible luminescence change in response to the EGFR inhibitor **1b**. A likely explanation for the inferior performance of probe **2g** compared to probe **2f**, even though they both possess electron-donating auxiliary substituents, is that the probes' interactions with the targeted biomolecules can be highly sensitive to differences in hydrophobicity, permeability and binding affinity

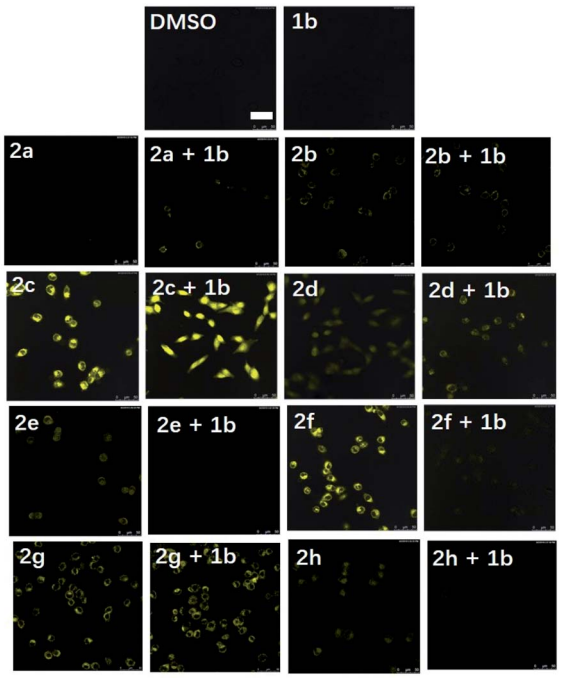

Fig. 3 Application of complexes **2a–2h** as luminescent probes for EGFR imaging in EGFR-overexpressing A431 human epidermoid carcinoma cells. Cells were treated with vehicle control (0.2% DMSO) or complexes **2a–2h** (1 μM) containing 0.2% DMSO for 2 h before imaging. The luminescence intensity was detected at ex/em = 405 nm/500–700 nm. Scale bar = 50 μm.

in living cells.[53–56] Moreover, previous studies have suggested that methoxy group played a key role in the interaction between several FDA-approved EGFR inhibitors (*e.g.* erlotinib, gefitinib, brigatinib and osimertinib) and EGFR.[57–60] In summary, although probes **2a–2h** all exhibited versatile photophysical characteristics and inhibition activity against EGFR, their sensing performance under the natural *in cellulo* environment was then considered as the crucial evaluation criterion for use as theranostic agents. Hence, **2f** was selected as the final candidate for further investigation due to its superior selectivity for EGFR in living cells.

To further support the hypothesis that complex **2f** bound to EGFR in cells, the cellular thermal shift assay (CETSA) was used to quantify the extent of drug engagement. Complex **2f** significantly stabilized EGFR in A431 cell lysates compared to the DMSO control (Fig. 4a), suggesting that complex **2f** engaged EGFR within cells to act as a luminescent probe. We next examined the selectivity of complex **2f** for EGFR over common biologically interfering substances, including common amino acids (Arg, His, Asp, Ser, Gln, Cys, Pro, Tyr and Trp), glutathione (GSH), glutathiol (GSSG), homocysteine, homocysteine, metal ions (Mg^{2+}, Fe^{3+}, Cu^{2+}, Al^{3+}, Na^{+}, K^{+}, Ca^{2+}, Zn^{2+}, Fe^{2+} and Mn^{2+}) and anions (S^{2-}, HCO_3^-, CO_3^{2-}, SO_3^{2-}, Cl^-, SO_4^{2-}, F^-, ClO_4^-, NO_3^-, HPO_4^{2-} and $H_2PO_4^-$) (Fig. S4†). The results indicated that complex **2f** was capable of sustaining a robust luminescent signal in the presence of commonly existing biological interfering substances. Stability assays revealed that complex **2f** was stable for at least seven days at 298 K, either in a DMSO-d_6/D_2O (9 : 1) solution or in an acetonitrile/H_2O (9 : 1) solution as verified by ^{1}H NMR spectroscopy (Fig. S5a†) or UV/Vis spectroscopy (Fig. S5b†), respectively, indicating its suitability for use in further imaging experiments. Overall, these results suggested that complex **2f** is a permanent "always-on" EGFR probe with excellent selectivity and stability.

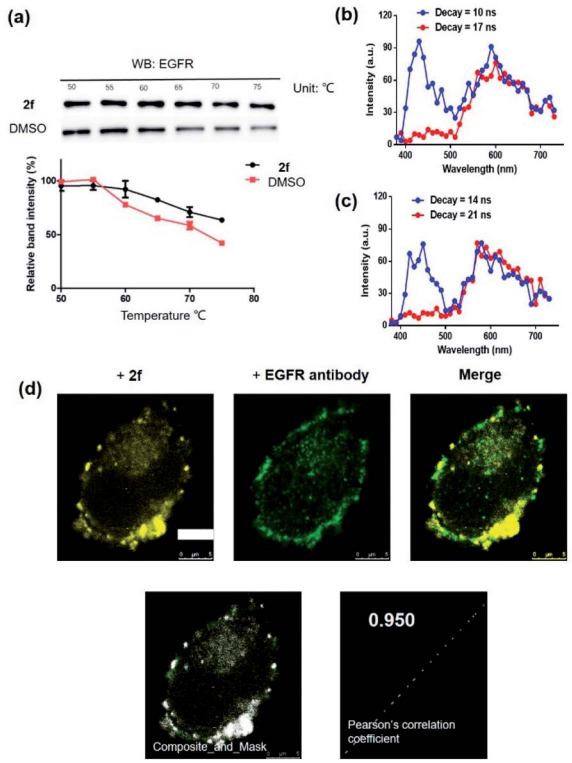

Fig. 4 (a) Effects of complex **2f** on the thermal stability of EGFR in cell lysates. A431 cells lysates were treated with **2f** (1 μM) for 1 h. Time-resolved spectra of complex **2f** (10 μM) in the presence of fluorescent organic dyes (b) thioflavin S (THS) and (c) coumarin 460 (Cm460) as two model matrix interferences to simulate the autofluorescence of biological samples in PBS buffer containing 1% DMSO. (d) Co-localization studies of complex **2f** (1 μM, 30 min) with EGFR protein in A431 cells. The Pearson's correlation coefficient of complex **2f** with EGFR protein was calculated to 0.950. ex/em = 405 nm/500–700 nm. Scale bar = 5 μm.

Compared with traditional organic dye-based probes, the long-lived lifetime of transition metal complex-based probes endows them with the competitive benefit of being able to discriminate their signal output even in a highly autofluorescent background. This hypothesis was verified for **2f** by evaluating its emission using TRES on a Horiba fluorescence spectrometer (FL3C-21).[61] Two fluorescent organic dyes, coumarin 460 (Cm460) and thioflavin S (THS), were selected as model matrix interferences to simulate the autofluorescence of biological samples with maximum emission at 460 nm and 428 nm, respectively. After 10 ns and 14 ns, which is before the completion of the fluorescence decay of THS or Cm460, respectively, the luminescence of complex **2f** was perturbed by the emission peaks of THS at 428 nm (Fig. 4b) and Cm460 at 460 nm (Fig. 4c), leading to reduced accuracy of measurement due to the undesirable interference of the signal output for EGFR. However, after the decay of 17 ns and 21 ns, which is after the completion of the fluorescence decay of THS or Cm460, respectively, the interfering signal from these dyes were almost completely eliminated, while the emission of complex **2f** was still retained with considerable intensity. In addition, we recorded the luminescence of complex **2f** alone at different decay times, and the spectra was identical to that in the presence of organic dyes after fluorescence decay was completed, further confirming that the observed time-resolved signals were due to complex **2f** (Fig. S6†). These results demonstrate the potential use of time-resolved techniques to discriminate the signal of **2f** in highly autofluorescent biological samples.

To explore whether the long lifetime of complex **2f** could be distinguished from background fluorescence *in cellulo*, we compared the emission of **2f** with a commercially-available cellular dye (4′,6-diamidino-2-phenylindole (DAPI)) in living A431 cells using TRES on a multi-mode microplate reader.[31,62] After incubating the cells with both complex **2f** and DAPI for 2 h, the signal output from the cells was recorded with the delay time set to 50 μs (Fig. S7a†) and 200 μs (Fig. S7b†), respectively. The results indicated the luminescence of complex **2f** could be readily distinguished from potentially interfering fluorescence using TRES. Taken together, complex **2f** exhibits a long-lived phosphorescence both *in vitro* and *in cellulo*, allowing for its potential for long-lived monitoring of EGFR in living systems *via* time-gated mode.

Many anticancer drugs have limited ability to discriminate between living normal and tumor cells, which can lead to low

efficacy and severe side effects. Given the ability of complex **2f** to engage EGFR *in vitro*, we next investigated whether complex **2f** could visualize EGFR in living cancer cells using a co-localization assay (Fig. 4d). Encouragingly, complex **2f** (1 μM) showed strong colocalization with EGFR protein in A431 cancer cells as detected *via* immunofluorescence. A high Pearson's correlation coefficient (Rr = 0.950) between the cell images was detected, suggesting that complex **2f** visualizes EGFR through selective binding to EGFR in cells. In order to further verify that complex **2f** interacts selectively with the targeted EGFR protein, imaging experiments were repeated in EGFR knockdown A431 cells (Fig. 5a). Notably, a noticeable decrease in the luminescence of **2f** was recorded in the EGFR knockdown group compared to untreated cells, suggesting the binding of complex **2f** to EGFR is required for the generation of luminescent signal output in A431 cells. Moreover, complex **2f** displayed much higher luminescence in A431 cells, which overexpress EGFR, than in normal human hepatocyte LO2 cells that expressed less EGFR (Fig. 5b). This result indicates that **2f** has potential for the real-time discrimination of cancer cells that overexpress EGFR compared to normal cells with lower EGFR expression.

Given the ability of complex **2f** to visualize EGFR in living cancer cells, we next explored the cytotoxicity of complex **2f** in either EGFR-overexpressing A431 cancer cells or normal LO2 cells. The 3-(4,5-dimethylthiazol-2-yl)-2,5-diphenyltetra-zolium bromide (MTT) assay was conducted by using the reference EGFR inhibitor **1b** as a positive control. Complex **2f** displayed comparable cytotoxicity against EGFR-overexpressing A431 cancer cells (IC_{50} = 37.40 ± 4.10 μM) compared to the reference EGFR inhibitor **1b** (IC_{50} > 50.0 μM) (Fig. S8a and b†). Many transition metal complexes exhibit inherent toxicity due to the metal center, may lead to reduced biocompatibility and undesired side effects due to the damage to healthy cells or tissues, which can limit their application as therapeutic drugs. Therefore, the cytotoxicity of **2f** was also investigated against normal LO2 cells. Encouragingly, complex **2f** was less toxic to LO2 cells (IC_{50} > 50.0 μM) (Fig. S8c and d†) compared to cancer cells. Taken together, these results suggested that complex **2f** possesses promising biocompatibility for theranostic applications.

Encouraged by the results above, we further studied the inhibitory activity of complex **2f** against EGFR *in vitro* and in living cancer cells. The *in vitro* biological potency of **2f** in suppressing the activity of EGFR was assessed with **1b** as a positive control by using a commercial EGFR kinase assay kit. The results showed that both complex **2f** and the positive control **1b** could reduce EGFR activity in a dose-dependent manner (Fig. 6a and b). Notably, complex **2f** inhibited EGFR activity with an EC_{50} value of 1.18 ± 0.09 μM, making it comparable to the positive control **1b** which had an EC_{50} value of 4.28 ± 0.22 μM. Taken together, these data indicated that **2f** could target and suppress the activity of EGFR *in vitro*.

The activation of EGFR triggers a cascade of phosphorylation events in the MEK/ERK pathway.[63] To investigate the ability of complex **2f** to inhibit downstream proteins in living A431 cells, the levels of P-ERK and P-MEK in the MEK/ERK pathway was measured by western blotting. Upon pre-incubation with **2f**, a significant decrease in the expression levels of P-ERK and P-MEK were recorded compared to the DMSO control, while no significant change on the expression levels of total ERK and MEK proteins were observed (Fig. 6c). The effects of **2f** on P-ERK and P-MEK expression were phenocopied by EGFR knockdown using siRNA (Fig. S9†). These results indicate that **2f** down-regulates the activation of downstream proteins including P-ERK and P-MEK in living A431 cells, *via* targeting EGFR. To

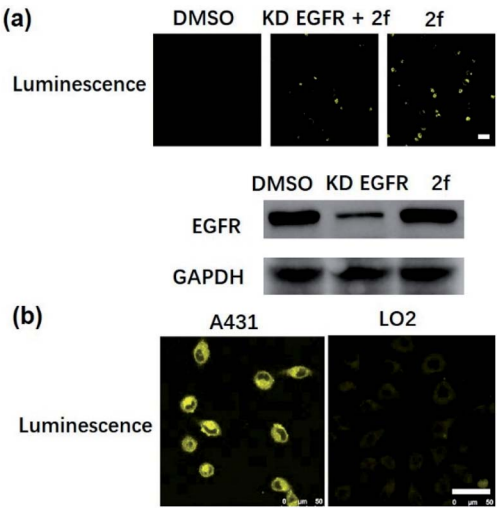

Fig. 5 (a) Confocal imaging of EGFR knockdown A431 cells. EGFR knockdown A431 cells were incubated with **2f** (1 μM) for 2 h at 37 °C. ex/em = 405 nm/500–700 nm. Scale bar = 50 μm. (b) Confocal imaging of normal LO2 cells and EGFR-overexpressing A431 cells. LO2 cells and A431 cells were incubated with **2f** (1 μM) for 2 h at 37 °C. ex/em = 405 nm/500–700 nm. Scale bar = 50 μm.

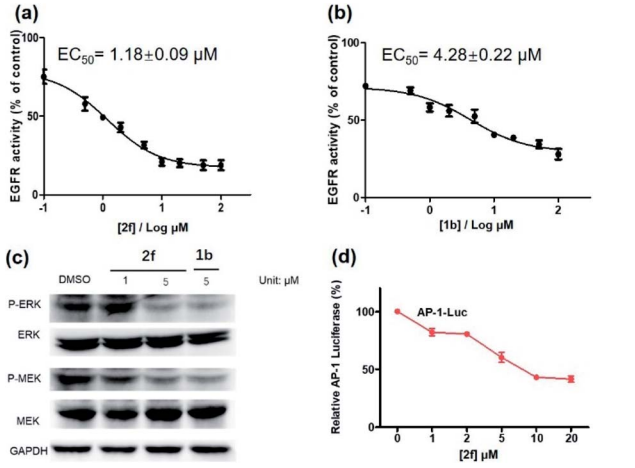

Fig. 6 EGFR inhibition activity of complex **2f** (a) and the reference inhibitor **1b** (b) in EGFR-overexpressing A431 cells. (c) Effects of complex **2f** and **1b** on P-ERK, ERK, P-MEK and MEK protein expression. A431 cells were treated with **2f** for 12 h. The protein levels were revealed by western blot assay. (d) Effects of complex **2f** on the transcription activity of downstream protein AP-1. A431 cells were transfected with AP-1 luciferase plasmid for 48 h, and then treated with **2f** at different concentration. AP-1 transcription activity was detected.

further explore the ability of complex **2f** to block the downstream effects of EGFR in A431 cells, a luciferase reporter assay was performed to evaluate the effect of **2f** on the activity of the transcription factor AP-1, a downstream target in the MEK/ERK pathway. Upon the increasing concentration of **2f**, the activity of AP-1 was reduced in a dose-dependent manner, suggesting that **2f** can decrease AP-1 transcription activity (Fig. 6d). Taken together, these results suggested that **2f** could suppress the activity of EGFR in living A431 cells to inhibit downstream pathways.

Conclusions

In summary, using a structure-guided design principle, we have validated our design concept by successfully developing a series of dual-functional iridium(III) complex based theranostic **2a–2h** for the simultaneously visualization and inhibition of EGFR in EGFR-overexpressing living cancer cells. A known EGFR inhibitor **1b** was grafted to an iridium(III) complex precursor **1a**, leading to the endowment of biological activity from the inhibitor while maintaining the desirable photophysical characteristics of the metal complex iridium(III). The properties of the iridium(III) complex-based theranostics were fine-tuned by the modification of auxiliary ligands with electron-withdrawing fluorine atoms (**2e**), electron-donating methyl (**2g**) or methoxy (**2f**) groups, different aromatic ring systems (**2a–2d**) or a sulfur-containing heterocycle (**2h**), generating a range of conjugates **2a–2h** that all exhibited increased EGFR inhibition activity compared to the known inhibitor **1b** while retaining desirable photophysical properties including long-lived lifetime, good stability, high quantum yield, and large Stokes shift. Unexpectedly, probe **2f** containing electron-donating methoxy groups on the "signaling unit", rather than the most luminescent counterpart **2c** or the most long-lived counterpart **2d**, was the most promising candidate after consideration of both *in vitro* and *in cellulo* performance. The candidate theranostic **2f** selectively bound to EGFR both *in vitro* and in living cells as revealed by a cellular thermal shift assay, a western blotting assay, a knockdown assay and a co-localization assay. The long-lived luminescence of **2f** in the sub-microsecond regime enabled its luminescence to be readily distinguished from the interfering fluorescence of fluorescent dyes by TRES. Remarkably, complex **2f** discriminated living EGFR-overexpressing cancer cells (A431 cells) from normal cells (LO2 cells) that express low level of EGFR with an "always-on" luminescence signal output. Moreover, complex **2f** inhibited the activity of EGFR in a dose-dependent manner, decreased the phosphorylation of downstream proteins ERK and MEK, and inhibited the activity of downstream transcription factor AP1. Notably, complex **2f** exhibited comparable inhibitory activity against EGFR with an EC_{50} value of 1.18 ± 0.09 μM compared to the parental EGFR inhibitor **1b** ($EC_{50} = 4.28 \pm 0.22$ μM) and caused a slightly higher cytotoxicity ($IC_{50} = 37.40 \pm 4.10$ μM) against EGFR-overexpressing A431 cancer cells. Taken together, these results demonstrate the promising potential of complex **2f** as an EGFR-selective dual-functional inhibitor and probe ("theranostic") in targeting living cancer cells. To our knowledge, this is the first small molecule-based iridium(III) theranostic for the simultaneous visualization and inhibition of EGFR in highly autofluorescent living cancer cells.

Experimental

Cellular thermal shift assay

Cellular thermal shift assay was performed to monitor the target engagement of **2f** in A431 cell lysates. Briefly, cell lysates from 2×10^6 A431 cells were collected, diluted in PBS and separated in the same aliquots. Each aliquot was treated with **2f** (10 μM) or DMSO 30 min after incubation at room temperature, the compound-treated lysates were divided into 50 μL in each of PCR tubes and heated individually at different temperatures (Veriti thermal cycler, Applied Biosystems/Life Technologies). The heated lysates were centrifuged and the supernatants were analyzed by SDS-PAGE followed by immunoblotting analysis by probing with the indicated antibody.

Immunofluorescence

The cells were initially washed for three times using phosphate-buffered saline (PBS) buffer. Afterwards, 4% PFA was added to the cells for incubation of 30 min, with following triplicate washing by PBS. Next, another 30 min of incubation is required by adding 0.5% Triton X-100 into cells at room temperature, followed by PBS washing for three times. After blocking with 5% BSA for 30 min, the cells were treated by the primary EGFR antibody for overnight incubation at 4 °C and subsequent treatment of the secondary antibody for 3 h at ambient temperature.

Western blotting

A431 cells were seeded at a density of 6×10^5 cell in a 6-well plate overnight. Cells were treated with vehicle control, EGFR inhibitor **1b**, or complex **2f** (in 0.1% DMSO) in 1% FBS medium for 12 h incubation. Cells were thereafter lysed to collect protein for each sample. Western blotting analysis was performed as described.

Knockdown assay

A431 cells were seeded in 6-well plate at 80% confluences in DMEM medium for 24 h incubation. EGFR siRNA (5′-GGCACGAGUAACAAGCUCAdTdT-3′ (sense), 5′-UGAGCUUGUUACUC GUGCCdTdT-3′ (antisense)) and Lipo3000 reagent were gently mixed and let for 20 min incubation at ambient temperature. Afterwards, the siRNA/Lipo3000 mixture (500 μL) was added into each well. Cells were next kept in a CO_2 incubator for 48 h post-transfection at 37 °C before further experiment.

Luciferase reporter assay

The inhibition of AP-1 activity was examined by a luciferase reporter assay (Promega, Madison, WI, USA). Briefly, A431 cells were seeded in a culture dish at a density of 6×10^5 cell for overnight incubation. AP-1-luciferase plasmid was next used to

co-transfect the cells using TurboFect Transfection Reagent in a serum-free DMEM medium. The transfected cells were subsequently seeded in a 24-well plate and followed by treatment of **2f** at indicated concentrations for 6 h in 1% FBS medium. Passive Lysis Buffer (PLB) (160 μL) was added into the transfected cells for lysis. Next, equal volume of luciferase reporter reagent (LAR) and the cell lysates (50 μL) were added and mixed in a 96-well plate. The transcriptional activity was thus measured by determining the activity of firefly luciferase in SpectraMax M5 microplate reader (Molecular Devices).

Conflicts of interest

There are no conflicts to declare.

Acknowledgements

This work is supported by Hong Kong Baptist University (FRG2/17–18/003), the Health and Medical Research Fund (HMRF/14150561), the National Natural Science Foundation of China (22077109 and 21775131), the Hong Kong Baptist University Century Club Sponsorship Scheme 2020, the Interdisciplinary Research Matching Scheme (RC–IRMS/16–17/03), Interdisciplinary Research Clusters Matching Scheme (RC–IRCs/17–18/03), Collaborative Research Fund (C5026–16G), SKLEBA and HKBU Strategic Development Fund (SKLP_1920_P02), the Science and Technology Development Fund, Macau SAR (File no. 0072/2018/A2), the University of Macau (MYRG2018–00187–ICMS and MYRG2019–00002–ICMS).

Notes and references

1 C. J. Adams and T. J. Meade, *Chem. Sci.*, 2020, **11**, 2524–2530.
2 T. Lammers, S. Aime, W. E. Hennink, G. Storm and F. Kiessling, *Acc. Chem. Res.*, 2011, **44**, 1029–1038.
3 K. Yang, L. Feng, X. Shi and Z. Liu, *Chem. Soc. Rev.*, 2013, **42**, 530–547.
4 J. D. Brown and A. G. Winterstein, *J. Clin. Med.*, 2019, **8**, 989.
5 J. Xie, S. Lee and X. Chen, *Adv. Drug Delivery Rev.*, 2010, **62**, 1064–1079.
6 J. V. Jokerst and S. S. Gambhir, *Acc. Chem. Res.*, 2011, **44**, 1050–1060.
7 Y. Xia, W. Li, C. M. Cobley, J. Chen, X. Xia, Q. Zhang, M. Yang, E. C. Cho and P. K. Brown, *Acc. Chem. Res.*, 2011, **44**, 914–924.
8 I. Brigger, C. Dubernet and P. Couvreur, *Adv. Drug Delivery Rev.*, 2012, **64**, 24–36.
9 L. Brannon-Peppas and J. O. Blanchette, *Adv. Drug Delivery Rev.*, 2004, **56**, 1649–1659.
10 D. Peer, J. M. Karp, S. Hong, O. C. Farokhzad, R. Margalit and R. Langer, *Nat. Nanotechnol.*, 2007, **2**, 751–760.
11 E.-K. Lim, T. Kim, S. Paik, S. Haam, Y.-M. Huh and K. Lee, *Chem. Rev.*, 2014, **115**, 327–394.
12 R. Liu, C. Hu, Y. Yang, J. Zhang and H. Gao, *Acta Pharm. Sin. B*, 2019, **9**, 410–420.
13 C. Chu, M. Su, J. Zhu, D. Li, H. Cheng, X. Chen and G. Liu, *Theranostics*, 2019, **9**, 3134.
14 C. Xu, F. Pu, J. Ren and X. Qu, *Chem. Commun.*, 2020, **56**, 5295–5298.
15 R. Kumar, W. S. Shin, K. Sunwoo, W. Y. Kim, S. Koo, S. Bhuniya and J. S. Kim, *Chem. Soc. Rev.*, 2015, **44**, 6670–6683.
16 S. Santra, C. Kaittanis, O. J. Santiesteban and J. M. Perez, *J. Am. Chem. Soc.*, 2011, **133**, 16680–16688.
17 E.-J. Kim, S. Bhuniya, H. Lee, H. M. Kim, C. Cheong, S. Maiti, K. S. Hong and J. S. Kim, *J. Am. Chem. Soc.*, 2014, **136**, 13888–13894.
18 Y. Yuan, R. T. Kwok, B. Z. Tang and B. Liu, *J. Am. Chem. Soc.*, 2014, **136**, 2546–2554.
19 R. Weinstain, E. Segal, R. Satchi-Fainaro and D. Shabat, *Chem. Commun.*, 2010, **46**, 553–555.
20 G. Nkepang, M. Bio, P. Rajaputra, S. G. Awuah and Y. You, *Bioconjugate Chem.*, 2014, **25**, 2175–2188.
21 H. Yuan, H. Chong, B. Wang, C. Zhu, L. Liu, Q. Yang, F. Lv and S. Wang, *J. Am. Chem. Soc.*, 2012, **134**, 13184–13187.
22 M. Bio, P. Rajaputra, G. Nkepang, S. G. Awuah, A. M. Hossion and Y. You, *J. Med. Chem.*, 2013, **56**, 3936–3942.
23 T. Zou, C. T. Lum, S. S. Y. Chui and C. M. Che, *Angew. Chem., Int. Ed.*, 2013, **52**, 2930–2933.
24 C. R. Cardoso, M. r. V. Lima, J. Cheleski, E. J. Peterson, T. Venâncio, N. P. Farrell and R. M. Carlos, *J. Med. Chem.*, 2014, **57**, 4906–4915.
25 R. R. Ye, Z. F. Ke, C. P. Tan, L. He, L. N. Ji and Z. W. Mao, *Chem.–Eur. J.*, 2013, **19**, 10160–10169.
26 V. Pierroz, T. Joshi, A. Leonidova, C. Mari, J. Schur, I. Ott, L. Spiccia, S. Ferrari and G. Gasser, *J. Am. Chem. Soc.*, 2012, **134**, 20376–20387.
27 D.-L. Ma, C. Wu, H. Liu, K.-J. Wu and C.-H. Leung, *J. Mater. Chem. B*, 2020, **8**, 3249–3260.
28 C. Wu, K.-J. Wu, J.-B. Liu, X.-M. Zhou, C.-H. Leung and D.-L. Ma, *Chem. Commun.*, 2019, **55**, 6353–6356.
29 Q. Zhao, C. Huang and F. Li, *Chem. Soc. Rev.*, 2011, **40**, 2508–2524.
30 M. Yu, Q. Zhao, L. Shi, F. Li, Z. Zhou, H. Yang, T. Yi and C. Huang, *Chem. Commun.*, 2008, 2115–2117.
31 T. C. O'Riordan, A. V. Zhdanov, G. V. Ponomarev and D. B. Papkovsky, *Anal. Chem.*, 2007, **79**, 9414–9419.
32 C.-N. Ko, G. Li, C.-H. Leung and D.-L. Ma, *Coord. Chem. Rev.*, 2019, **381**, 79–103.
33 V. Venkatesh, R. Berrocal-Martin, C. J. Wedge, I. Romero-Canelón, C. Sanchez-Cano, J.-I. Song, J. P. C. Coverdale, P. Zhang, G. J. Clarkson, A. Habtemariam, S. W. Magennis, R. J. Deeth and P. J. Sadler, *Chem. Sci.*, 2017, **8**, 8271–8278.
34 A. B. Caballero, L. Cardo, S. Claire, J. S. Craig, N. J. Hodges, A. Vladyka, T. Albrecht, L. A. Rochford, Z. Pikramenou and M. J. Hannon, *Chem. Sci.*, 2019, **10**, 9244–9256.
35 K. K.-W. Lo, *Acc. Chem. Res.*, 2020, **53**, 32–44.
36 C. Wang, Z. Wang, T. Zhao, Y. Li, G. Huang, B. D. Sumer and J. Gao, *Biomaterials*, 2018, **157**, 62–75.
37 L. G. Meimetis, J. C. Carlson, R. J. Giedt, R. H. Kohler and R. Weissleder, *Angew. Chem., Int. Ed.*, 2014, **53**, 7531–7534.
38 P. Saraon, J. Snider, Y. Kalaidzidis, L. E. Wybenga-Groot, K. Weiss, A. Rai, N. Radulovich, L. Drecun, N. Vučković, A. Vučetić, V. Wong, B. Thériault, N.-A. Pham, J. H. Park,

A. Datti, J. Wang, S. Pathmanathan, F. Aboualizadeh, A. Lyakisheva, Z. Yao, Y. Wang, B. Joseph, A. Aman, M. F. Moran, M. Prakesch, G. Poda, R. Marcellus, D. Uehling, M. Samaržija, M. Jakopović, M.-S. Tsao, F. A. Shepherd, A. Sacher, N. Leighl, A. Akhmanova, R. Alawar, M. Zerial and I. Stagljar, *Nat. Chem. Biol.*, 2020, **16**, 577–586.

39 Y. Jia, C. M. Quinn, S. Kwak and R. V. Talanian, *Curr. Drug Discovery Technol.*, 2008, **5**, 59–69.

40 M. Gao, F. Yu, C. Lv, J. Choo and L. Chen, *Chem. Soc. Rev.*, 2017, **46**, 2237–2271.

41 S. Arounaguiri and B. G. Maiya, *Inorg. Chem.*, 1999, **38**, 842–843.

42 K. Y. Pu, K. Li and B. Liu, *Adv. Funct. Mater.*, 2010, **20**, 2770–2777.

43 C. Wu, K. Vellaisamy, G. Yang, Z.-Z. Dong, C.-H. Leung, J.-B. Liu and D.-L. Ma, *Dalton Trans.*, 2017, **46**, 6677–6682.

44 K. Vellaisamy, G. Li, C.-N. Ko, H.-J. Zhong, S. Fatima, H.-Y. Kwan, C.-Y. Wong, W.-J. Kwong, W. Tan and C.-H. Leung, *Chem. Sci.*, 2018, **9**, 1119–1125.

45 H. Kobayashi, M. Ogawa, R. Alford, P. L. Choyke and Y. Urano, *Chem. Rev.*, 2010, **110**, 2620–2640.

46 W. Wang, C. Yang, S. Lin, K. Vellaisamy, G. Li, W. Tan, C. H. Leung and D. L. Ma, *Chem.–Eur. J.*, 2017, **23**, 4929–4935.

47 A. Gazit, P. Yaish, C. Gilon and A. Levitzki, *J. Med. Chem.*, 1989, **32**, 2344–2352.

48 J. S.-Y. Lau, P.-K. Lee, K. H.-K. Tsang, C. H.-C. Ng, Y.-W. Lam, S.-H. Cheng and K. K.-W. Lo, *Inorg. Chem.*, 2008, **48**, 708–718.

49 S. M. King, S. Claire, R. I. Teixeira, A. N. Dosumu, A. J. Carrod, H. Dehghani, M. J. Hannon, A. D. Ward, R. Bicknell, S. W. Botchway, N. J. Hodges and Z. Pikramenou, *J. Am. Chem. Soc.*, 2018, **140**, 10242–10249.

50 A. Kazama, Y. Imai, Y. Okayasu, Y. Yamada, J. Yuasa and S. Aoki, *Inorg. Chem.*, 2020, **59**, 6905–6922.

51 E. C. Glazer, D. Magde and Y. Tor, *J. Am. Chem. Soc.*, 2005, **127**, 4190–4192.

52 D. Magde, M. D. Magde and E. C. Glazer, *Coord. Chem. Rev.*, 2016, **306**, 447–467.

53 M. T. Jarlstad Olesen, R. Walther, P. P. Poier, F. Dagnæs-Hansen and A. N. Zelikin, *Angew. Chem., Int. Ed.*, 2020, **132**, 7460.

54 D. Zhang, Y. Huang, X. You, L. Wang, G. Zhang, S. Gui, Y. Jin and R. Zhao, *Angew. Chem., Int. Ed.*, 2020, **132**, 10128.

55 C. Mattsson, T. Andreasson, N. Waters and C. Sonesson, *J. Med. Chem.*, 2012, **55**, 9735–9750.

56 C. Mattsson, T. Andreasson, N. Waters and C. Sonesson, *J. Med. Chem.*, 2013, **56**, 4130–4133.

57 R. Tjin Tham Sjin, K. Lee, A. O. Walter, A. Dubrovskiy, M. Sheets, T. S. Martin, M. T. Labenski, Z. Zhu, R. Tester, R. Karp, A. Medikonda, P. Chaturvedi, Y. Ren, H. Haringsma, J. Etter, M. Raponi, A. D. Simmons, T. C. Harding, D. Niu, M. Nacht, W. F. Westlin, R. C. Petter, A. Allen and J. Singh, *Mol. Cancer Ther.*, 2014, **13**, 1468–1479.

58 M. Cichocki, H. Szaefer, V. Krajka-Kuźniak and W. Baer-Dubowska, *Mol. Cell. Biochem.*, 2014, **396**, 221–228.

59 L. Yang, S. Ying, S. Hu, X. Zhao, M. Li, M. Chen, Y. Zhu, P. Song, L. Zhu, T. Jiang, H. An, N. A. Yousafzai, W. Xu, Z. Zhang, X. Wang, L. Feng and H. Jin, *Signal Transduction Targeted Ther.*, 2019, **4**, 25.

60 S.-H. I. Ou, J. Cui, A. B. Schrock, M. E. Goldberg, V. W. Zhu, L. Albacker, P. J. Stephens, V. A. Miller and S. M. Ali, *Lung Cancer*, 2017, **108**, 228–231.

61 C. Zhang, M. Liu, S. Liu, H. Yang, Q. Zhao, Z. Liu and W. He, *Inorg. Chem.*, 2018, **57**, 10625–10632.

62 R. I. Dmitriev, H. M. Ropiak, G. V. Ponomarev, D. V. Yashunsky and D. B. Papkovsky, *Bioconjugate Chem.*, 2011, **22**, 2507–2518.

63 S. Meloche and J. Pouysségur, *Oncogene*, 2007, **26**, 3227–3239.